DEVELOPMENT OF A PARITY VIOLATION EXPERIMENT FOR UNDERGRADUATE LABORATORIES

By

Josiah C. Kratz

A thesis submitted in partial fulfillment of the
requirements for the degree of

Bachelor of Arts

Houghton College

May 2020

Signature of Author……..
Department of Physics
May 19, 2020

……
Dr. Mark Yuly
Professor of Physics
Research Supervisor

……
Dr. Brandon Hoffman
Professor of Physics

DEVELOPMENT OF A PARITY VIOLATION EXPERIMENT FOR UNDERGRADUATE LABORATORIES

By

Josiah C. Kratz

Submitted to the Department of Physics
on May 11, 2020 in partial fulfillment of the
requirement for the degree of
Bachelor of Arts

Abstract

An undergraduate experiment is being developed at Houghton College to measure weak nuclear parity violation. Parity violation, discovered in 1956-57 by Lee and Yang [1], and Wu [2], was a breakthrough in modern physics, but has yet to make its way into undergraduate laboratories. Following a method originally suggested by Lee and Yang, a coincident counting experiment is being developed to measure the transmission through magnetized iron of circularly polarized gamma rays from ^{60}Co beta decay. A BGO gamma detector and silicon beta detector, collinear on either side of a ^{60}Co source with a steel electromagnet core between the source and gamma detector, measure the gamma rays in coincidence with the beta particles. Since the Compton scattering cross section in the magnetized steel depends on the relative orientations of the gamma ray spin and the spin of the polarized electrons in the magnet, an asymmetry in the transmission count rate when the magnet is polarized in opposite directions demonstrates that parity is violated.

Thesis Supervisor: Dr. Mark Yuly
Title: Professor of Physics

TABLE OF CONTENTS

TABLE OF FIGURES

Chapter 1

INTRODUCTION TO EXPERIMENT

1.1. Introduction

An experiment is being developed at Houghton College to observe parity violation in weak nuclear interactions, with the goal being to develop a simple and inexpensive procedure that could be carried out on the undergraduate level. Despite being a monumental discovery of modern physics, parity violation experiments are not typically part of the standard undergraduate or graduate nuclear physics curriculum, so the hope is that by developing a low-cost experiment with a simple procedure, this significant discovery will finally be made more accessible to undergraduate students.

1.2. Prediction of Parity Violation

Until the 1950's, physicists believed that the four fundamental forces, the weak, strong, electromagnetic, and gravitational forces, all conserved parity, meaning that their interactions were the same under a spatial inversion in three dimensions. Thirty years prior, it had been experimentally shown that both the strong and electromagnetic forces conserve parity, and for that reason it was assumed that the weak force also conserves parity [1]. In fact, parity conservation was thought to be just as fundamental as the conservation laws of energy, momentum, and electric charge [3].

In 1956, physicists struggled with what they called the "theta-tau puzzle" [4]. It appeared that there were two types of K mesons, a type of subatomic particle which can decay by weak interactions. One K meson, at that time called the theta meson, decayed into two pi mesons. The other K meson, which at that time was called the tau meson, decayed into three pi mesons. Both types of K mesons had identical mass, charge, and lifetime, suggesting that they were the same particle. However, the theta meson has even parity, while its decay particle, the pi meson, has odd parity. Two pi mesons have a total parity that is even, meaning that parity is conserved during the decay of the theta meson. However, because it was assumed that parity is conserved during weak decay reactions,

physicists were forced to conclude that there was a second particle, the tau meson, which had odd parity, which would allow for a decay of three pi mesons.

At a nuclear physics conference at the University of Rochester the so called "theta-tau puzzle" was discussed, and it was suggested that maybe parity was violated by the weak force, offering a simple solution to the problem. Although no one could point specifically to evidence conflicting with the suggestion, most physicists found this answer inconceivable. Tsung Dao Lee and Chen Ning Yang were in attendance at the meeting, and the following summer studied past experimental results regarding weak interactions [4]. To their surprise, they found no evidence for parity conservation. As a result, they thought of several definitive tests which could show if parity was conserved in weak interactions [1]. Despite there being no evidence to support parity conservation, Richard Feynman echoed the general feelings of the physics community when he placed a fifty-dollar bet that parity would be shown to be conserved [3].

1.3. Parity transformation

In order to test parity conservation, a system must be measured before and after a parity transformation. If the system is different after the parity transformation, then parity symmetry has been violated. As shown in Figure 1, a parity transformation inverts the directions of the x, y, and z coordinate axes, resulting in a transformation from a right-handed coordinate system to a left-handed coordinate system or vice versa. The same result can be reached by inverting the system itself instead of the coordinate system. As expected, two parity transformations done on the same system restore that coordinate system to its original state. A parity transformation can also be completed by a mirror transformation, followed by a rotation of 180^{o}. For this reason, in many cases including this experiment, the important feature is changing a right-handed coordinate system into a left-handed system, and so a parity transformation can be thought of as equivalent to a mirror transformation.

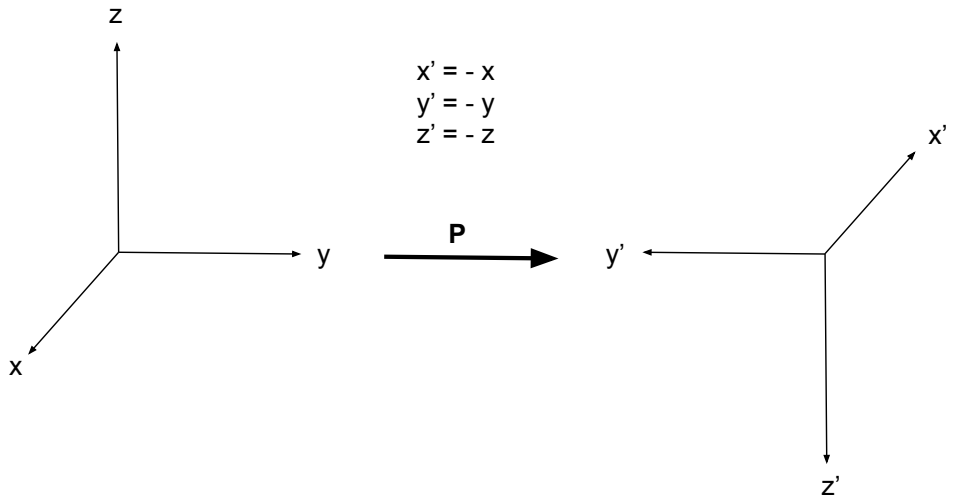

Figure 1. The system undergoes a parity transformation P. The directions of the x, y, and z coordinate axes are all inverted, resulting in a transformation from a right-handed coordinate system to a left-handed coordinate system or vice versa.

As an example of parity conservation, consider angular momentum, $\boldsymbol{L}$, is:

$$\boldsymbol{L} = \boldsymbol{r} \times \boldsymbol{p}, \tag{1}$$

where $\boldsymbol{r}$ is the position vector, and $\boldsymbol{p}$ is the linear momentum. Completing a parity transformation on the system inverts both the position and momentum:

$$\boldsymbol{L} = -\boldsymbol{r} \times -\boldsymbol{p}. \tag{2}$$

Equations (1) and (2) are identical, showing that the angular momentum remains unchanged after a parity transformation, thus angular momentum conserves parity.

1.4. Possible experiments to demonstrate parity violation

As mentioned before, both the strong and electromagnetic forces had been shown to exhibit parity symmetry, and because of this it was assumed for several decades that the weak force exhibited this property as well. T. D. Lee and C. N. Yang were the first to point out that this assumption had no basis in experimental evidence, and proposed four ways this assumption could be tested [1].

One of the ways Lee and Yang suggested was to use beta decay, which is the result of weak interactions in the nucleus, and occurs in a nucleus when a neutron changes to a proton or vice versa, resulting in a more stable nucleus. One convenient beta source to use for testing parity violation is ^{60}Co. This unstable isotope of Cobalt undergoes beta minus decay, in which a neutron decays into a proton and emits a beta particle (electron) and an antineutrino. The resulting daughter nucleus is an excited state of ^{60}Ni, which then de-excites via gamma ray emission. As shown in Figure 2, the most probable decay path of ^{60}Co emits an electron, two gamma rays, and an antineutrino.

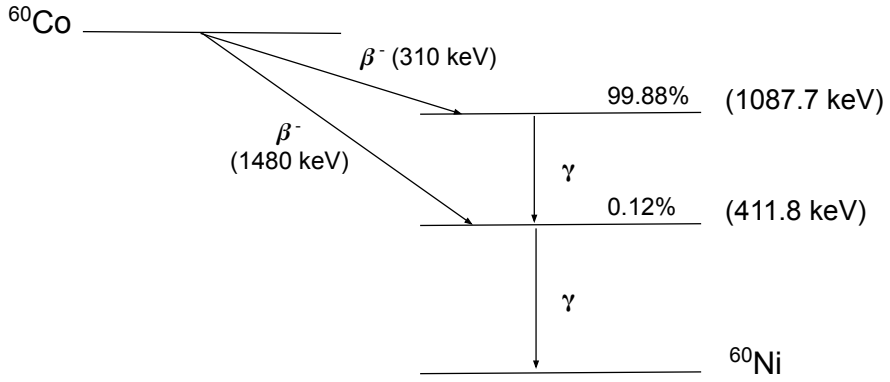

Figure 2. Energy level diagram for beta minus decay of ^{60}Co into ^{60}Ni. The most probable decay path emits beta particle and antineutrino, followed by two gamma rays.

One possible experiment suggested by Lee and Yang involved measuring the angular distribution of electrons coming from the beta decay of oriented nuclei. A measured asymmetry in the number of decay products detected between θ and $180^0 - \theta$ (where θ is the angle between the spin of the ^{60}Co nucleus and the momentum of the beta particle) would show that parity is violated by the weak force [1].

A second possible experiment suggested by Lee and Yang involves measuring the circular polarization of gamma rays emitted by a nucleus during beta decay. A photon is circularly polarized if its spin is aligned or anti-aligned with the direction of its momentum. In this beta-gamma correlation experiment, the gamma rays detected must be un-polarized if parity is conserved [1]. If there is a net circular polarization of the emitted gamma rays, in which gamma rays are emitted preferentially in one direction with respect to the spin of the decaying ^{60}Co nucleus, then it would be shown that parity is violated. This is because a

circular polarization of gamma rays means there is preferential direction in which beta particles are emitted in the decay.

1.5. History and Development of Apparatus

1.5.1. Wu experiment

To test one of the propositions of Lee and Yang, in 1957 Chien-Shiung Wu conducted the first experiment [2] testing for parity violation by studying the electrons emitted by the beta decay of ^{60}Co. As shown in Figure 3, Wu polarized the ^{60}Co nuclei by cooling the nuclei in a cryostat in the presence of an applied magnetic field created by a solenoid. As a result, the nuclear spins aligned with the applied magnetic field, and became polarized. To measure the degree of polarization of the ^{60}Co source, NaI scintillation counters were placed in both the equatorial plane and polar direction. Because the direction of the emitted gamma rays is correlated to the direction of the magnetic moment of the ^{60}Ni nucleus, an observed anisotropy of emitted gamma rays can be used to measure the degree of polarization of the nuclei. To detect the beta particles, a thin anthracene crystal was placed above the source. Beta particles emitted from the source hit the anthracene and caused scintillations which were transmitted through a glass window and a clear plastic Lucite light pipe to a photomultiplier located on top of the cryostat.

Wu recorded beta and gamma counts for the two different directions of the applied magnetic field (upward and downward). By doing so, Wu essentially performed a parity transformation on the system. If the beta particles were emitted preferentially in a certain direction relative to the nuclear spin, then it would be shown that parity is violated by the system. Wu's results are shown in Figure 4. The top plot shows the gamma anisotropy as it changes over time, measured using the NaI gamma detectors. The difference in count rate between the equatorial and polar counters shows that the nuclei are indeed polarized. As time progresses and the temperature increases, the polarization goes to zero as expected. The bottom plot shows the measured beta asymmetry for when the external magnetic field is in opposite directions. Astoundingly, Wu found that more electrons were emitted in the direction opposite the nuclear spin than those that were emitted in the same direction.

Again, as expected, the asymmetry went to zero at the same time the nuclei became unpolarized.

These results were the first to show that beta decay, a process brought about by the weak force, does not conserve parity. As a result of this remarkable discovery, Lee and Yang were awarded the 1957 Nobel Prize in Physics [5], and Wu was awarded the Wolf Prize [6].

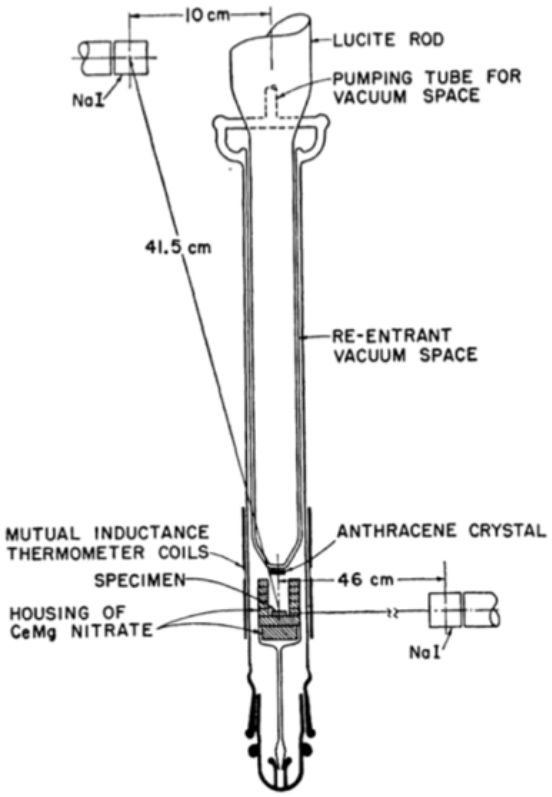

Figure 3. Schematic drawing of the experimental apparatus used in Wu's experiment. Beta particles emitted by the source were detected by the anthracene crystal scintillator, and gamma rays emitted were detected by the two NaI detectors. Figure taken from Ref. [2].

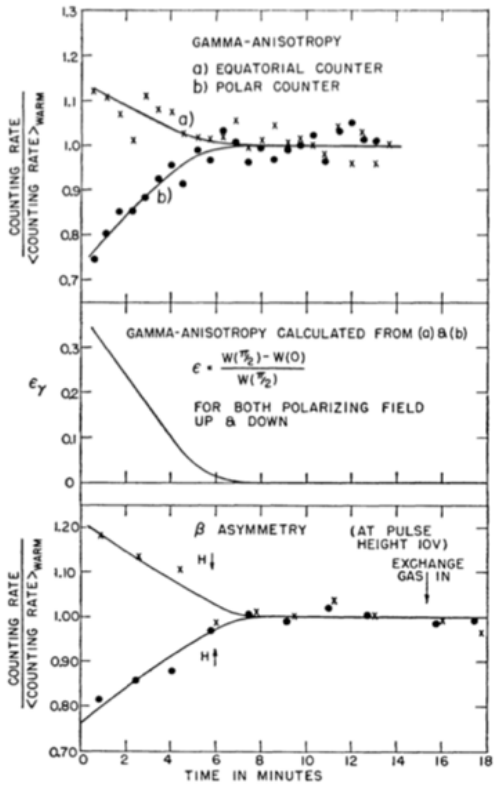

Figure 4. Wu's results showing the gamma anisotropy and beta asymmetry in her experiment. The gamma anisotropy (top) was used to measure the degree of polarization of the nuclei. The beta asymmetry (bottom) was measured when the magnetic field was in opposite directions. As time elapsed, the temperature increased, resulting in the depolarization of the nuclei. As expected, the beta asymmetry and gamma anisotropy went to zero at the same time. The figure was taken from Wu's original paper [2].

1.5.2. Lundby et al. Experiment

Following Wu's remarkable discovery, A. Lundby, A. Patro, and J.-P. Stroot developed a similar experiment [7] that confirmed the parity violation of the weak force. In this experiment, Lundby et al. used an unpolarized ^{60}Co source and measured the beta-gamma coincidence rate for circularly polarized gamma rays traveling through magnetized iron in both directions of electron polarization. By doing so, they were able to indirectly measure the number of beta particles emitted relative to the spin of the ^{60}Co nucleus. As shown in Figure 5, Lundby placed the ^{60}Co source against an iron absorber that formed the core of a magnet, which polarized the electrons in the iron. Above the absorber was a NaI crystal acting as a gamma ray detector, and directly below the source was an anthracene crystal

acting as a beta detector. The light from both crystals was coupled to a photomultiplier tube (PMT) by light guides in order to keep the PMT's away from the magnetic field.

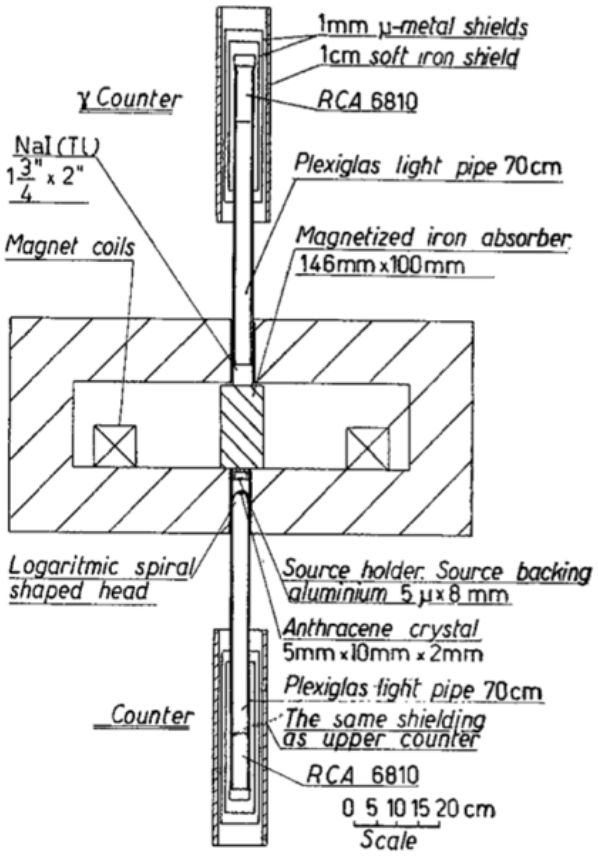

Figure 5. Schematic drawing of the experimental apparatus used in the Lundby et al. experiment. Beta particles emitted by the source were detected using the anthracene crystal scintillator, and gamma rays were detected using the NaI detector. Gamma rays had to first travel through a magnetized iron absorber, in which they were transmitted with different probabilities depending on their circular polarization. Figure taken from Ref. [7].

By only recording coincidence events, Lundby et al. ensured that the gamma rays were from the same decay that emitted a beta particle in the opposite direction, and were therefore circularly polarized. Because the transmission rate of the emitted gamma rays through the iron depends on the relative orientation of the circular polarization of the gamma rays and the spin of the electrons, if parity symmetry was violated, then there would be a difference in count rate when the magnet was polarized in opposite directions.

Indeed, they found an asymmetry in the number of counts detected with each direction of magnet polarization, confirming Wu's result that parity is violated.

1.6. Introduction to and Motivation for the Experiment at Houghton College

The experiment being developed at Houghton College is similar to the Lundby et al. experiment. Because their experiment did not require the polarization of nuclear spins, a similar experiment can be constructed without the need of expensive cryogenic equipment. The experimental setup at Houghton is shown schematically in Figure 6. A ^{60}Co source is between a cylindrical beta detector and a cylindrical electromagnet. A gamma detector, placed along the symmetry axis, is positioned collinearly on the other side of the electromagnet. If a difference in the coincidence count rate is measured by the detectors when the magnet is polarized in opposite directions, then it has been shown that parity has been violated.

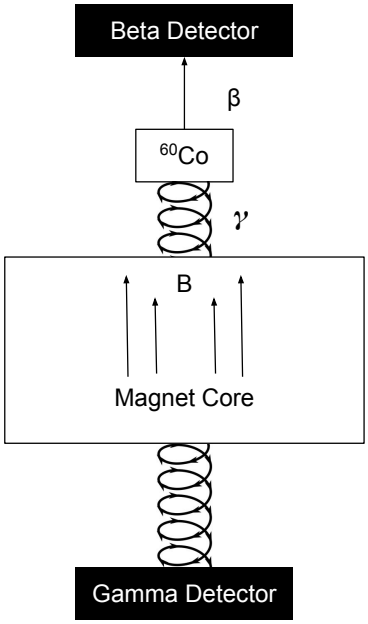

Figure 6. Simplified diagram of the apparatus at Houghton College. The ^{60}Co source is positioned between the magnetized core and the beta detector, with the gamma detector on the other side of the magnet. Circularly polarized gamma rays emitted opposite from beta particles were attenuated by the steel magnet core.

As far as can be determined, there has been no development of a parity violation experiment which measures the asymmetry in this way. For this reason, a low-cost coincidence experiment that demonstrates the parity violation of the weak force is being studied. The goal is that this apparatus can be assembled by students using equipment common in an undergraduate physics lab. The hope is that this design can be incorporated into the undergraduate physics curriculum, making parity violation phenomena more accessible to undergraduate students.

Chapter 2

THEORY

2.1. Introduction

The experiment developed at Houghton college measures the degree of circular polarization of gamma rays emitted from ^{60}Co. In the first part of this chapter, angular momentum conservation will be analyzed for the ^{60}Co nucleus, leading to the circular polarization of gamma rays emitted opposite coincident beta particles. The degree of circular polarization can be measured using the transmission rate of gamma rays through magnetized steel. In the next part of the chapter, it will be shown how the Compton scattering cross section in the magnetized steel depends on the relative orientations of the gamma ray spin and the spin of the polarized electrons in the magnet. Hence an asymmetry in the transmission count rate when the magnet is polarized in opposite directions indicates that the source is polarized. Finally, it will be shown how this measured polarization gives an asymmetry which demonstrates parity violation.

2.2. Beta Decay of ^{60}Co

The beta minus decay of ^{60}Co will be utilized to study parity violation in this experiment. As shown in Figure 7, ^{60}Co is an unstable isotope which undergoes beta minus decay, in which a neutron decays into a proton and emits a beta particle (electron) and an antineutrino,

$$^{60}\mathrm{Co} \rightarrow {}^{60}\mathrm{Ni} + \beta^{-} + \overline{\nu}_{e}. \qquad (3)$$

The resulting daughter nucleus is an excited state of ^{60}Ni, which then de-excites by emitting either one or two gamma rays,

$$^{60}\mathrm{Ni}^{*} \rightarrow {}^{60}\mathrm{Ni} + \gamma_1 + \gamma_2. \qquad (4)$$

The most probable decay path (99.88%) of ^{60}Co emits an electron with an endpoint energy of 0.31 MeV, two gamma rays with energies of 1.1732 MeV and 1.3325 MeV, and an antineutrino. The other decay path (0.12%) emits a higher energy electron with an

endpoint energy of 1.48 MeV, a single gamma ray with an energy of 1.3325 MeV, and an antineutrino.

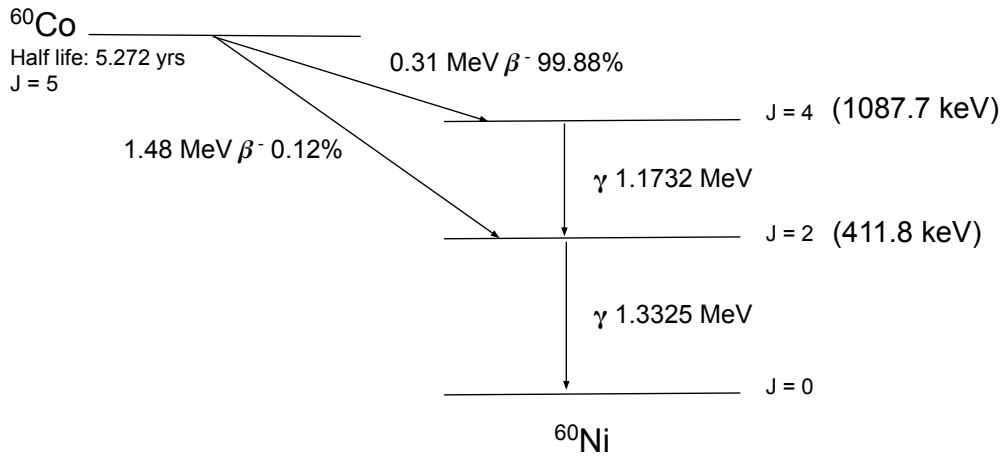

Figure 7. Decay scheme of ^{60}Co, with a half-life of 5.272 years. The majority (99.88%) of beta particles emitted have an endpoint energy of 0.31 MeV, resulting in the subsequent emission of two gamma rays with energies of 1.1732 MeV and 1.3325 MeV from the excited ^{60}Ni nucleus. A small percentage (0.12%) of the beta particles emitted have a much higher endpoint energy of 1.48 MeV, resulting in the emission of only a single gamma ray with an energy of 1.3325 MeV. Data taken from Ref. [8].

The total energy released is approximately equal to the mass difference between the parent and daughter nucleus. This energy is shared by the electron, neutrino, and residual nucleus, resulting in a beta energy spectrum from zero to the endpoint energy, in which the beta particle has nearly all the released energy. The average energy of the emitted beta particles is 95.77 keV for the more probable decay path (99.88%), and 625.87 keV for the less probable decay path (0.12%) [8].

The experiment is possible because the ^{60}Co nucleus decays into a "stretched state", meaning that the z-components of spin angular momentum of all the decay particles must point in the same direction to conserve angular momentum. Hence, the spins of the ^{60}Ni nucleus, the electron, and the antineutrino must point in the same direction as the original ^{60}Co spin. Since ^{60}Co has a spin of 5, both the electron and antineutrino have a spin of $\frac{1}{2}$, and the excited ^{60}Ni nucleus has a spin of 4, to conserve angular momentum the spins must be aligned as shown in Figure 8. Moreover, the spins of the gamma rays must also be in the

same direction as the original ^{60}Co spin. The two gamma rays emitted therefore both have a spin of 2, leaving a ground state ^{60}Ni nucleus with spin 0.

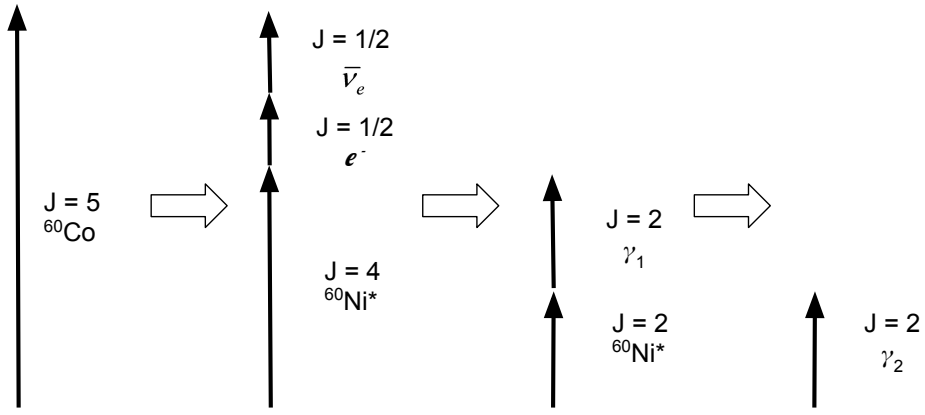

Figure 8. To conserve angular momentum, the spins of all of the decay particles must be aligned. The ^{60}Co nucleus has a spin of 5, which decays to an excited state of ^{60}Ni by emitting an antineutrino and an electron, each with a spin of $\frac{1}{2}$. The ^{60}Ni then emits two gamma rays, each with spin 2, resulting in a ground state ^{60}Ni nucleus of spin 0.

The conservation laws of momentum, spin, and helicity place additional restrictions on the ^{60}Co decay. The antineutrino must have right-handed helicity, meaning its spin always points in the direction of its momentum. The spin of the gamma rays must either be parallel or antiparallel to their momentum. The spin and momentum of the ejected beta particle however can be in any orientation. When these constraints on the particles momentum and spin are considered, several important conclusions can be made which are useful for parity violation experiments. Considering that the spins must also all point in the same direction allows for only two possible arrangements that can be detected by collinear beta and gamma detectors (Figure 9), either the beta particle is emitted with its spin aligned with its momentum and the gamma rays emitted with its spin opposite of its momentum or vice versa.

As shown in Figure 9, a left-handed beta particle, one in which the spin vector and velocity vector are antiparallel resulting in a negative helicity value, is always emitted opposite a right-handed gamma ray, one in which the spin vector and momentum vector are parallel, resulting in a positive helicity value for the beta particle. Because momentum and helicity

are conserved, by measuring the angular momentum of one decay particle, the momentum of the opposite particle can be determined. Thus, if in ^{60}Co an asymmetry can be measured in the number of left-handed and right-handed gamma rays emitted opposite a beta particle, it therefore indicates an asymmetry in the number of right-handed and left-handed beta particles.

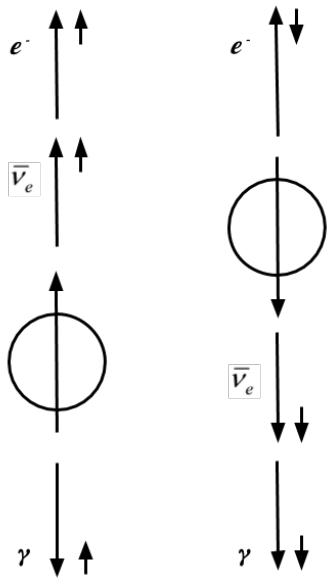

Figure 9. The detectable decay states of ^{60}Co. The beta particle is emitted either with its spin aligned with its momentum and the gamma ray emitted with its spin opposite of its momentum or vice versa. In both cases the antineutrino is emitted with its spin in the same direction as its momentum.

2.3. Demonstrating Parity Violation in ^{60}Co

Measuring an asymmetry in the decay rate of left-handed and right-handed gamma rays therefore allows for the determination of whether or not ^{60}Co beta decay violates parity. As previously mentioned, a parity transformation can be visualized as the mirror image of a system. As shown in Figure 10, if the spin of a left-handed beta particle is envisioned as a left-handed screw, in which the particle's spin is antiparallel to the direction of its motion, then a mirror transformation results in a right-handed screw, in which the particle's spin is in the direction of its motion.

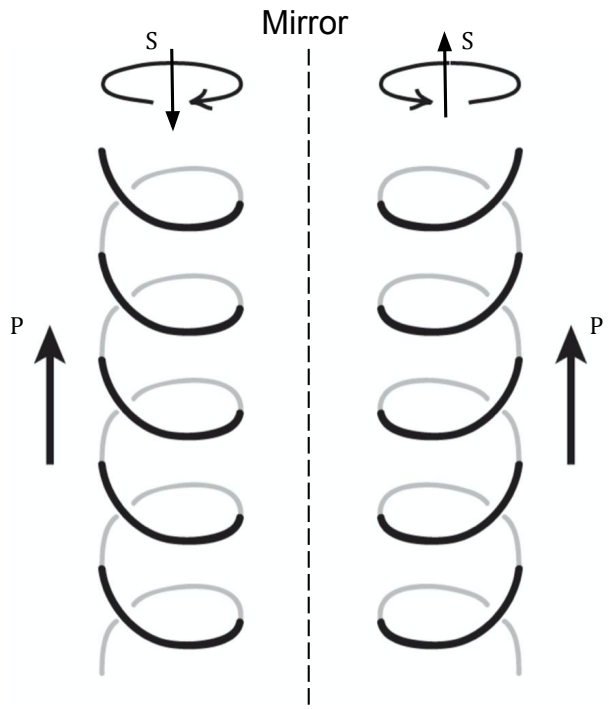

Figure 10. Mirror transformation of a screw. A mirror transformation of a left-handed screw (left-handed beta particle), in which the spin (S) and momentum (P) are antiparallel, transforms it into a right-handed screw (right-handed beta particle), in which the spin and momentum are parallel.

Similarly, a mirror transformation of the ^{60}Co nuclear spin in which the beta particle and gamma ray are ejected antiparallel to each other, results in the transformation shown in Figure 11. A right-handed beta particle is transformed into a left-handed beta particle, and a left-handed gamma ray is transformed into a right-handed gamma ray. The experiment at Houghton College, which utilizes collinear beta and gamma detectors, is designed to measure this scenario. Notice that this is exactly the scenario of the Wu experiment, but with aligned nuclear spin selected by the gamma coincidence requirement rather than a polarized source.

If parity is conserved, then there will be no way to distinguish between the system and its mirror image, so an equal number of left-handed and right-handed beta particles should be emitted from ^{60}Co. If however, an asymmetry is measured in the number of beta particles emitted parallel or antiparallel to the direction of the spin of the ^{60}Co nucleus, then parity has been shown to be violated. As shown in this section, measuring an asymmetry in the

number of right-handed and left-handed gamma rays indicates an asymmetry in the decay rate into right-handed and left-handed beta particles. Because an asymmetry in the number of right-handed and left-handed beta particles demonstrates that parity has been violated, measuring the asymmetry in the emission rate of circularly polarized gamma rays in the opposite direction is one way to experimentally test if parity is indeed violated.

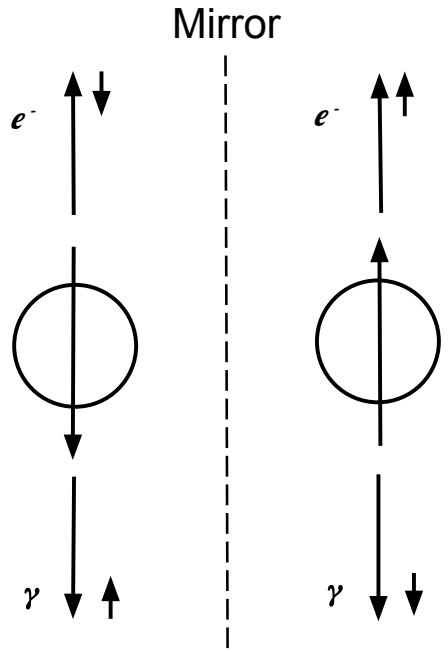

Figure 11. Mirror transformation of the ^{60}Co decay. The beta particle is transformed from right handed to left handed, and the gamma ray is transformed from left handed to right handed.

2.4. Expected count rate of experiment

Gamma radiation following a beta decay is circularly polarized if emitted parallel or antiparallel to the emitted electron [9]. Circular polarization of gamma rays can be detected by observing the interaction of the gamma rays with a magnetized material, in which the electrons' spins are aligned. As a result, an asymmetry in the emission of right-handed and left-handed gamma rays can be measured by making the gamma rays first pass through a magnetized steel absorber before they reach the detector. The gamma rays have different

probabilities of Compton scattering with the electrons in the magnetized steel depending on the alignment of the spins of the gamma rays and the electrons relative to each other.

For non-magnetized materials, the transmitted intensity, I, of gamma rays passing through iron is given by:

$$I = I_0 e^{-\mu x}, \tag{5}$$

where I_0 is the initial intensity, μ is the linear attenuation coefficient, and x is the distance traveled through the absorber. The linear attenuation coefficient is specific to the material, in this case steel, and depends on the energy of the gamma ray. One important contributor to the attenuation of the gamma rays is Compton scattering, in which gamma rays scatter from atomic electrons. The attenuation coefficient is therefore a function of the Compton scattering cross section.

The cross section is proportional to the probability of a scattering event occurring between two particles. For a photon and an electron, the differential scattering cross section can be written as [9],

$$d\sigma = \frac{{r_0}^2}{2}\left(\frac{k}{k_0}\right)^2 \{\phi_0 + P_1\phi_1 + fP_c\phi_c\}, \tag{6}$$

where r_0 is the classical electron radius, defined as,

$$r_0 = \frac{1}{4\pi\varepsilon_0}\frac{e^2}{m_e c^2}, \tag{7}$$

where e is the elementary charge, m_e is the electron mass, c is the speed of light, and ε_0 is the permittivity of free space. The initial and final momentum of the photon are $\boldsymbol{k_0}$ and $\boldsymbol{k}$, respectively, P_1 is the degree of linear polarization, P_c is the degree of circular polarization of the photon, and f is the fraction of oriented electrons. The ordinary Compton cross section, ϕ_0, is,

$$\phi_0 = 1 + \cos^2\vartheta + (k_0 - k)(1 - \cos\vartheta), \tag{8}$$

where ϑ is the scattering angle. Both ϕ_1 and ϕ_c depend on the polarization of the photons, where ϕ_1 is,

$$\phi_1 = \sin^2\vartheta, \tag{9}$$

and ϕ_c is,

$$\phi_c = -(1-\cos\vartheta)[(k_0 + k)\cos\vartheta\cos\psi + k\sin\vartheta\sin\psi\cos\varphi], \tag{10}$$

where ψ is the angle between the direction of the incident photon $\boldsymbol{k_0}$ and the electron spin $\boldsymbol{s}$, and φ is the angle between the $(\boldsymbol{k_0}\,\boldsymbol{k})$-plane and the $(\boldsymbol{ks})$-plane. As can be seen in Equation (10), the probability of an incident gamma ray scattering off an electron depends on ψ, the angle between the electron spin and momentum of the gamma ray. If the direction of the electron spin is reversed $(\psi + \pi)$, then there will be a difference in the number of gamma rays transmitted through the steel.

The asymmetry, which is the relative difference in count rate, E, when the electron spin is parallel vs. antiparallel to the incident gamma ray is [9]:

$$E = \frac{N_- - N_+}{(N_- + N_+)/2}, \tag{11}$$

where N_+ and N_- are the number of gamma rays transmitted with positive and negative magnet polarity, respectively.

Following the derivation of Ref. [10], it can be shown that the expected asymmetry is:

$$E = 2P_0 \tanh\left(\frac{N_a \rho P v \sigma_c x}{A}\right), \tag{12}$$

where N_a is Avogadro's number, A is the atomic mass of the material, ρ is its mass density, v is the number of oriented electrons per atom, and P is the polarization of gamma rays. Lundby et al. measured P_0 to be 0.6 for ^{60}Co where $P_0 = (N_R - N_L)/(N_R - N_L)$, and N_R and N_L are the number of right-handed and left-handed gamma rays, respectively. The polarization-sensitive correction factor for the differential cross section, σ_c, is given by Chesler [11] as,

$$\sigma_c = 2\pi r_0 \left\{ \frac{1 + 4k_0 + 5k_0^2}{k_0(1 + 2k_0)^2} - \frac{1 + k_0}{2k_0^2} \ln(1 + 2k_0) \right\}, \quad (13)$$

where $k_0 = E_\gamma / m_e c^2$, in which E_γ is the energy of the incident gamma ray, and $m_e c^2$ is the rest energy of an electron.

The expected collection time, T, for a specific detector geometry as a function of attenuator length x and target uncertainty $\delta E/E$ is,

$$T = \left(\frac{1}{P_0^2 \tanh^2(P v \sigma_c x)} - 1 \right) \frac{e^{\mu \rho x}}{\left(\frac{\delta E}{E}\right)^2 R_0 \cosh(n P v \sigma_c x)}, \quad (14)$$

where $n = N_a \rho / A$, and R_0 is the count rate for the same geometry but without the attenuator material, expressed as $R_0 = (N_R + N_L)/T$.

2.5. Magnetic Hysteresis

The magnet used in our experiment is an electromagnet, consisting of a solenoid wrapped around a steel core. When current is applied to the solenoid, the wire loops produce a magnetic field inside the solenoid. The strength of the magnetic field, H, is approximately:

$$H = \frac{NI}{L}, \quad (15)$$

where N is the number of turns of the coil, I is the applied current, and L is the length of the coil. As a result, the applied current is directly proportional to the strength of the magnetic field H.

Normally, the individual magnetic dipole moments of the atoms (mostly due to unpaired electron spins) making up a ferromagnetic material are randomly aligned, resulting in no net magnet field. However, when ferromagnetic material is placed inside a solenoid, the magnetic dipole moments of the iron atoms align. The magnetic flux density, $\boldsymbol{B}$, is:

$$\boldsymbol{B} = \mu_0(\boldsymbol{H} + \boldsymbol{M}), \quad (16)$$

where μ_0 is the permeability of free space and $\boldsymbol{M}$ is the magnetization, which is the net magnetic dipole moment per unit volume. For small fields, the magnetization is approximately linear, such that:

$$\boldsymbol{M} = \chi \boldsymbol{H}, \tag{17}$$

where χ is the magnetic susceptibility. The magnetic flux density then becomes:

$$\boldsymbol{B} = \mu \boldsymbol{H}, \tag{18}$$

where $\mu = \mu_0(1 + \chi)$. As more and more dipoles align with the magnetic field, the steel eventually becomes saturated, that is, it reaches a fixed value where all the unpaired electron spins are aligned.

When working with ferromagnets, it is important to note that they exhibit hysteresis. Generally, hysteresis is the dependence of the state of a system on its history. For an electromagnet, this means that the total magnetic field, $\boldsymbol{B}$, will not necessarily be the same given the same applied current, I, because the total magnetic field also depends on what the current was previously. This is a result of the magnetization, $\boldsymbol{M}$, of the iron being aligned in a certain way and requiring energy to realign, and so resisting a change in field strength. Consequently, the applied field must overcome the opposing field due to the iron as it switches polarity. This phenomenon is illustrated in the typical hysteresis curve pictured in Figure 12.

For the parity violation experiment discussed here, it is important that the magnetization, and hence **B**, be exactly the same magnitude when switching polarity in order to compare the count rate. The easiest way to achieve opposite polarity is by allowing the electromagnet to reach saturation, in which the magnetic moments of the iron atoms completely align in either orientation. If the magnet is not allowed to reach saturation, then care must be taken to develop a procedure to ensure that the magnetic field reaches the exact opposite polarity.

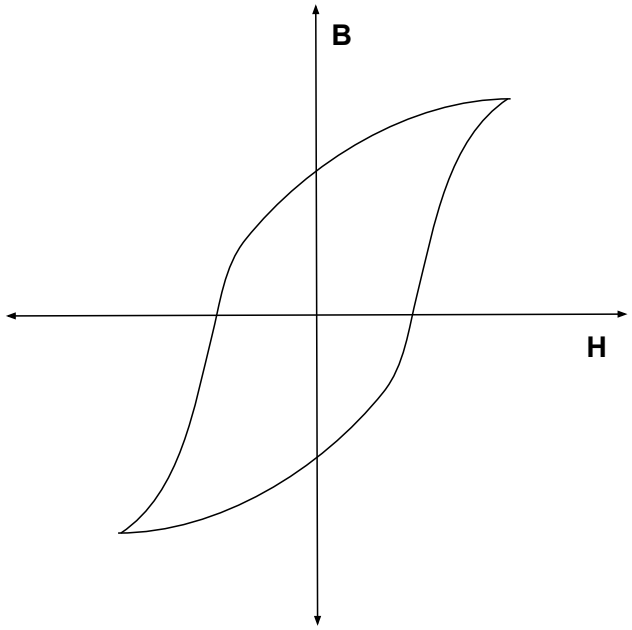

Figure 12. General magnetic hysteresis curve exhibited by a ferromagnetic material. As the external magnetic field, **H**, increases with current, so does the total magnetic field, **B**. When **H** decreases, **B** does not decrease at the same rate as it increased due to resistance from the aligned magnetic moments of the iron core.

Chapter 3

APPARATUS DESIGN AND EXPERIMENTAL PROCEDURE

3.1. Introduction

In this chapter, the physical apparatus and the proposed experimental procedure to measure the parity violation of the weak force will be discussed. The experiment being developed at Houghton College, similar to the Lundby et al. experiment, does not require the polarization of nuclei, and so does not need the expensive cryogenic equipment utilized in Wu's experiment. The experimental design uses two detectors to measure the asymmetry, as shown in Figure 6. A silicon surface barrier detector is used to detect beta particles, with the ^{60}Co source directly below it. An electromagnet with a steel core is placed between the source and the Bismuth Germanate (BGO) gamma detector. The source, both detectors, and the magnet are all collinear. The steel core of the electromagnet is magnetized along the axis through the two detectors and the source. Nuclear Instrumentation Modules (NIM) process coincident pulses from the beta and gamma detectors. Coincident and singles events were recorded using multichannel analyzers (MCA). A difference in coincident count rate when the magnet is polarized in opposite directions demonstrates parity violation.

3.2. Apparatus

Figure 13 is a drawing of the cylindrically symmetric apparatus, with an actual photograph of the apparatus shown in Figure 14. The silicon detector, ^{60}Co source, magnetized steel rod, and BGO detector were all collinear. The detectors and magnet were centered using acrylic rings. Lead shielding surrounds the BGO gamma detector to minimize outside background radiation. Aluminum foil surrounded the source and Si detector to ensure that it was light tight. The BGO detector was constructed using three 2" x 2" x 0.5" BGO crystals placed vertically side by side on top of an RCA 8575 photomultiplier tube (PMT) and 265 base, attached using silicone optical grease. To make light tight, crystals were wrapped in aluminum foil, and then covered in black electrical tape. A photograph of the detector is shown in Figure 15. A Magnetech R-6030-24 electromagnet was used to magnetize the

steel rod, and was powered using a TC 959 high voltage power supply. The magnet had a diameter of 15.2 cm. The steel plate on the bottom of the magnet had a thickness of 9.4 mm and the plate on the top had a thickness of 6.8 mm. The height of the steel rod was 7.7 cm, with a diameter of 2.5 cm, and a density of 7.15 $g \cdot cm^{-3}$.

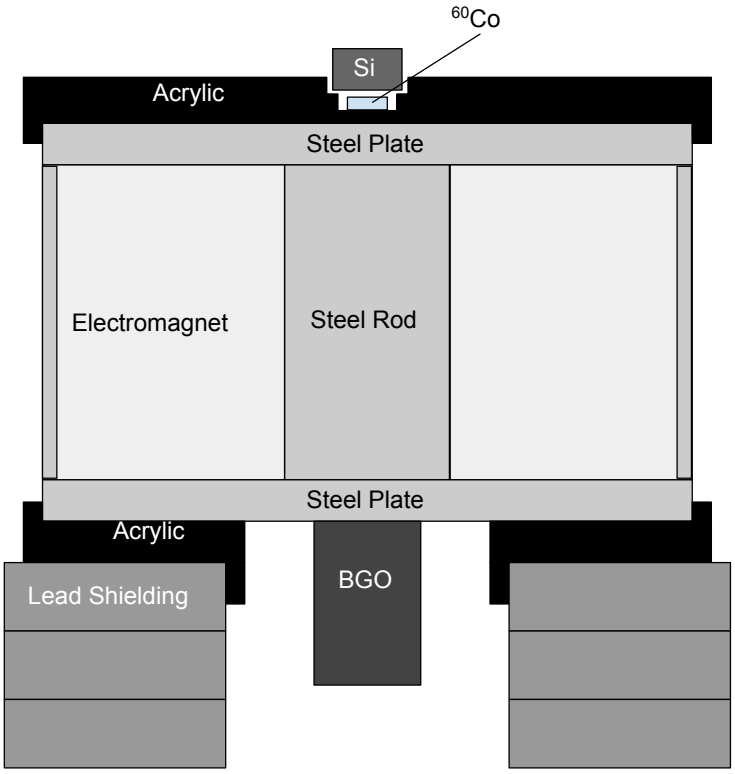

Figure 13. Cross section diagram of the physical apparatus. The Si detector, source, steel rod, and BGO detector are all collinear, held in place by an acrylic ring. Lead shielding surrounds the BGO detector to minimize accidental counts from the environment.

The source was prepared approximately six years ago by electroplating about 1 μC of ^{60}Co from a $CoCl_2$ solution onto stainless-steel foil, which was then glued to two thin polyethylene disks, each with a diameter of 13 mm and thickness of 0.8 mm, one on either side of the foil. Each disk had a 5 mm hole which allowed for the source to be directly exposed to the silicon detector.

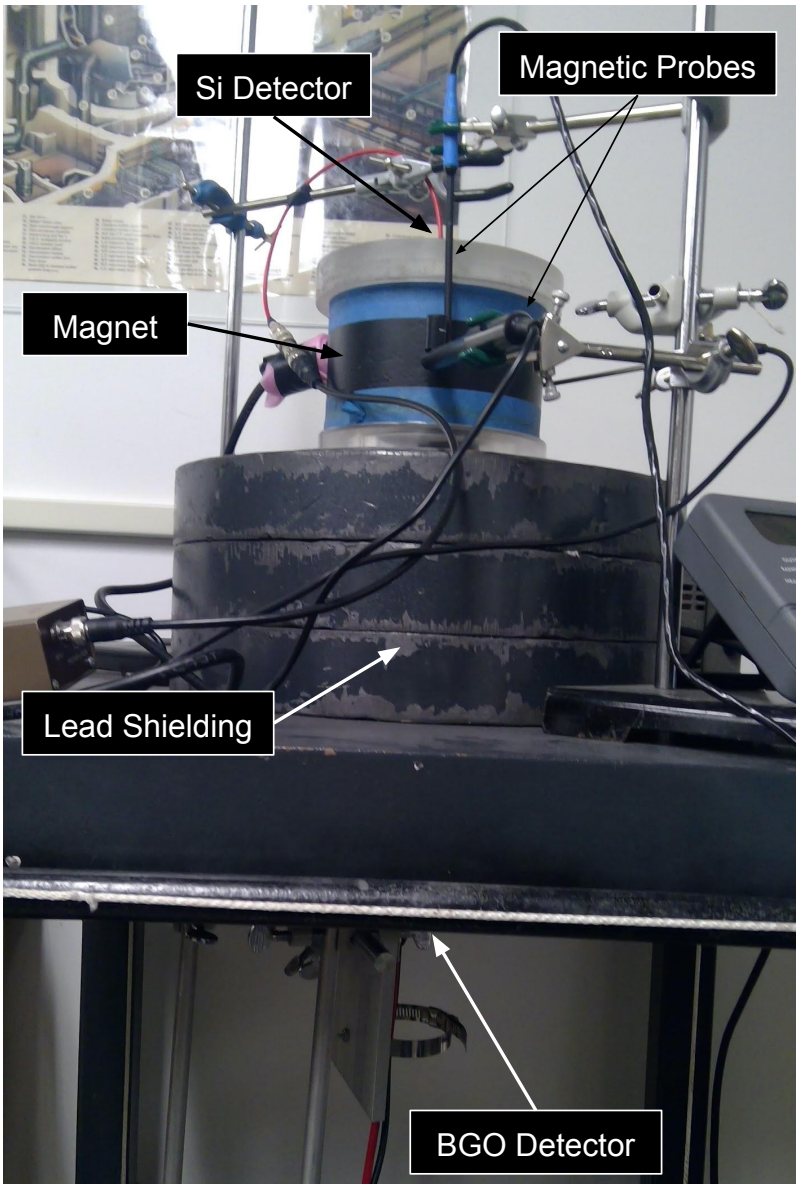

Figure 14. Photograph of apparatus. The ^{60}Co source (not visible) sits immediately below the Si detector. The magnet is between the source and the BGO detector, which cannot be seen because it is surrounded by lead shielding.

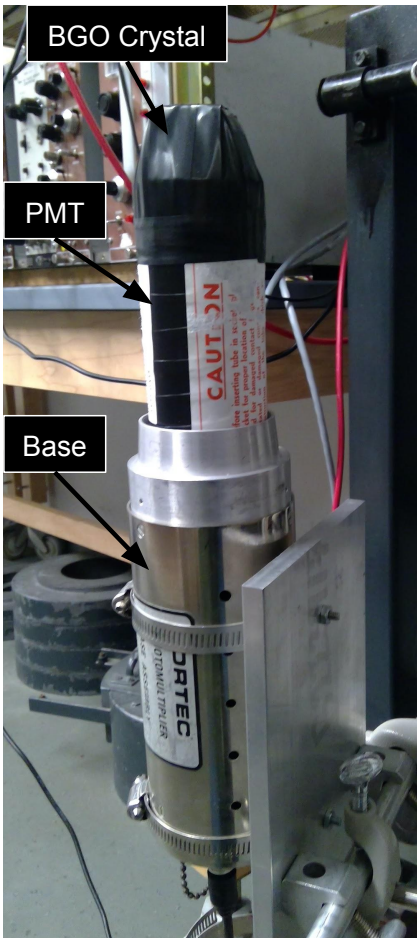

Figure 15. Photograph of the assembled BGO detector without the light guide. The BGO crystal was attached to the photomultiplier tube (PMT) using optical grease, which was attached to the base. To make the detector light tight, the BGO crystal was wrapped in foil, and the crystal was then held to the PMT using black electrical tape.

3.3. Electronics

Figure 16 shows the electronics used to process the pulses from the detectors. The silicon surface barrier detector (Ortec BA-014-025-1000) was biased to +180 V using an Ortec 428 power supply. It had an active area of 25 mm^2 and a minimum depletion depth of 1 mm. A surface barrier detector is a semiconductor with a p-n junction diode. The reverse bias applied to the diode forms a depletion region, a region in which there are no mobile charge carriers, with sufficient depth so that incident charged particles can stop within. When a beta particle enters the depletion region, it transfers energy to the semiconductor and

excites electrons, which creates electron-hole pairs which are free to move in the depletion region. The resulting current pulse is detected, with the total charge being proportional to the energy lost by the incoming particle. To ensure that beta pulses were indeed being detected, a beta spectrum of the source was taken using an Ortec 485 amplifier and SpecTech UCS-30 MCA 1. The MCA records the number of events per input channel. The different channels correspond to different peak energies, and the spectrum can be calibrated to determine the energy of the peaks. An Ortec 454 timing filter amplifier (TFA) was used to amplify and differentiate the pulses coming from the Ortec 142 pre-amplifier and an Ortec 437A constant fraction discriminator (CFD) provided a logic pulse for every pulse from the TFA that was above a moveable threshold voltage. By changing the threshold, the system could be triggered only on pulses large enough to be from beta particles.

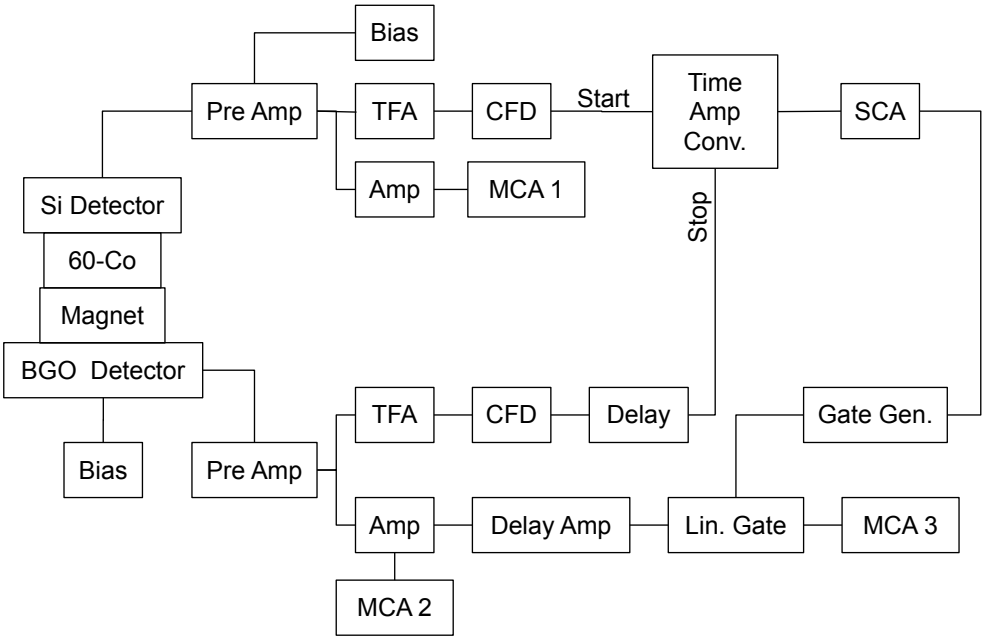

Figure 16. Electronics block diagram used to select coincident pulses. Each block represents a separate NIM module. The time to amplitude converter only allows gamma pulses through that coincide with beta pulses.

The BGO gamma detector was operated at -2000 V using an Ortec 428 bias supply. To ensure that gamma pulses were indeed being detected, a gamma spectrum of the source was taken using an Ortec 485 amplifier and SpecTech UCS-30 MCA 2. The BGO detector is a

scintillator detector. Atoms in the BGO crystal absorb energy from incident gamma rays and emit visible and ultraviolet light as they de-excite. The emitted light travels to the PMT and ejects electrons by the photoelectric effect. These electrons are accelerated through a series of dynodes to amplify the pulse. The voltage peak output from the detector is proportional to the energy of the incoming gamma ray. Similar to the beta detector, an Ortec 113 pre-amplifier, Ortec 454 TFA, and Ortec 437A CFD were used to shape the pulses and trigger on only gamma rays, producing a logic pulse for every event above the set threshold. An Ortec 467 time to amplitude converter (TPHC) was used to create a gate to select only gamma pulses that were detected in coincidence with beta pulses. The TPHC produced an analog pulse with height proportional to the time difference between the start and stop logic inputs. The start input was triggered by the output of the CFD from beta pulses, and the stop was triggered by the output of the CFD from gamma pulses. An Ortec 467 single channel analyzer (SCA) was used to select pulses within a certain pulse height, to select only the coincidence peak. The logic output of the SCA then entered an Ortec 416A gate generator before entering a Canberra 1451 linear gate.

The linear gate selected only gamma pulses that fell within the width of the gate produced by the gate generator, which was produced by coincident gamma and beta particles. As a result, only coincident gamma pulses were recorded by SpecTech UCS-30 MCA 3. The total count rate of the 1.17 and 1.33 MeV gamma peaks will be compared when the magnet is polarized in opposite directions.

3.4. Magnet Control

To switch the polarity of the magnet, an AMF KHU17D11 relay is used. When a threshold voltage is applied to the relay switch, it throws the switch and reverses the connection of the terminals of the power supply to the magnet, which switches the direction of the current through the magnet. The reversal of the direction of current through the electromagnet reverses the polarity of the magnet. However, due to hysteresis effects in the steel core, this does not exactly reverse the polarity of the magnet. This can be overcome by decreasing the current and then oscillating it around zero before increasing the current in the opposite direction.

The double pole double throw configuration is used in the AMF KHU17D11 (Figure 17). In this configuration, the voltage applied to the electromagnet across the 13 and 14 pins switches the direction of current through the magnet. When the threshold voltage is reached, the switch from pin 1 to pin 9 and pin 4 to pin 12 is opened, while the switch from pin 5 to pin 9 and pin 8 to pin 12 is closed, resulting in the direction of the current applied to the electromagnet being reversed. The current applied to the electromagnet and the voltage applied to the relay are both set using the computer controlled power supply.

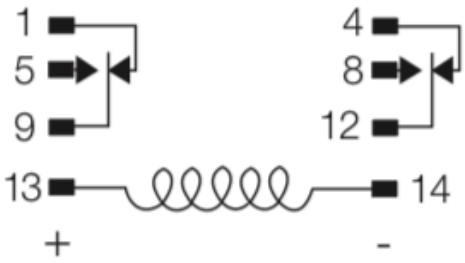

Figure 17. Circuit diagram of the double pole double throw configuration of the AMF KHU17D11 relay switch. The relay switch is used to switch the direction of the current applied to the electromagnet. Figure taken from Ref. [12].

Chapter 4

RESULTS

4.1. Introduction

Before coincidence data could be taken and a parity asymmetry could be measured, it was important to confirm that the electronics were working as expected, and that coincident events were a result of true events and accidental background. In addition, the beta and gamma singles count rates were roughly measured as well as the count rate of the coincidence experiment.

4.2. Timing Resolution

The timing resolution is an important parameter of the experiment. The higher the timing resolution, the higher the precision of the coincidence measurement. The TPHC outputs a voltage proportional to the time difference between the start and stop pulses. To calibrate the time difference, a LeCroy 2323A Gate/Delay Generator Camac module was used to apply a known length of delay between gamma pulses from the CFD entering the start and the stop inputs of the TPHC. The SpecTech UCS-30 MCA recorded the output of the TPHC for several seconds with a specific delay length applied, resulting in the formation of a sharp peak. The delay length was then changed, and the new resulting peak was recorded. Delay lengths of 50, 100, 200, 300, and 380 nanoseconds were used, resulting in the calibration plot shown in Figure 18. Next, the circuit was returned to the configuration shown in Figure 16, except the magnet was removed to increase the coincident count rate, and a NaI detector was used to record gamma pulses. The output of the TPHC from this setup was recorded for three hours using an MCA. The result was a calibrated histogram of the timing difference of coincident events, shown in Figure 19. The full width half max was 98 nanoseconds, meaning, on average, coincident pulses came within 98 nanoseconds of each other.

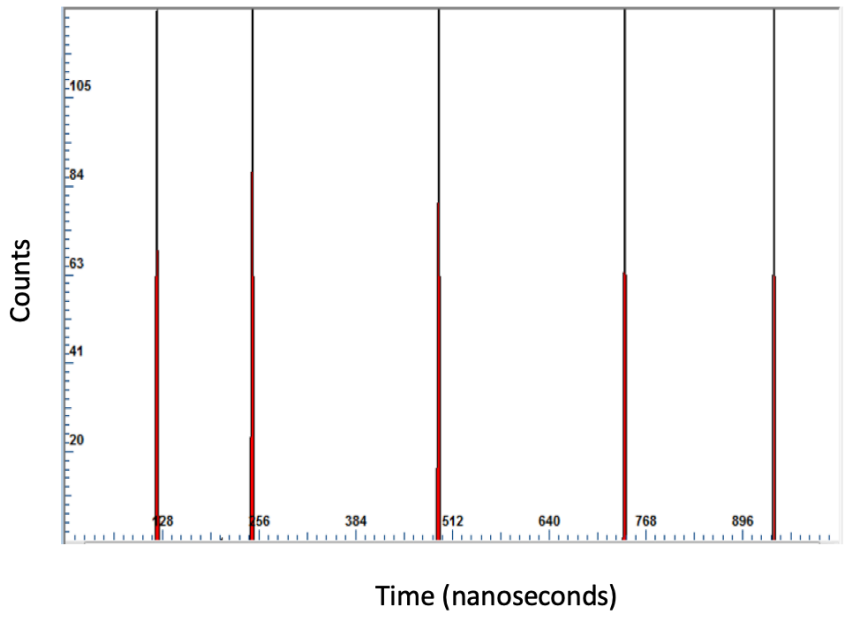

Figure 18. Calibration spectrum for the voltage output of the TPHC. From left to right, the delay amount is 50, 100, 200, 300, and 380 nanoseconds.

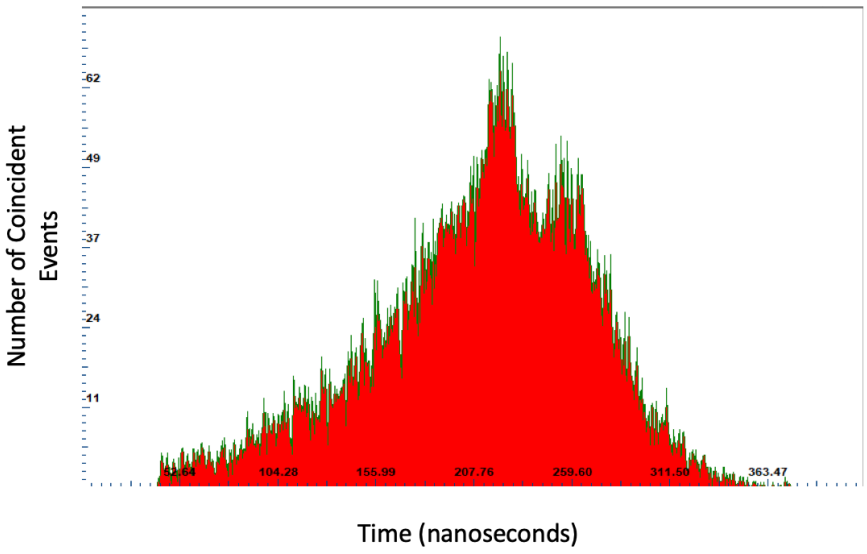

Figure 19. Calibrated histogram of the timing difference of coincident beta and gamma pulses. This is the output of the TPHC recorded using an MCA. The full width half max is 98 nanoseconds.

At the center of the peak is the highest probability that the counts recorded will be true coincident events. The farther away from the peak, the higher the probability that the event

will be an accidental. To eliminate a high fraction of these accidentals, a SCA is used to select for only the peak, as shown in Figure 20. The accidental rate was found to be approximately 0.135 counts per nanosecond, meaning for a FWHM of 98 nanoseconds approximately 14 accidentals were recorded.

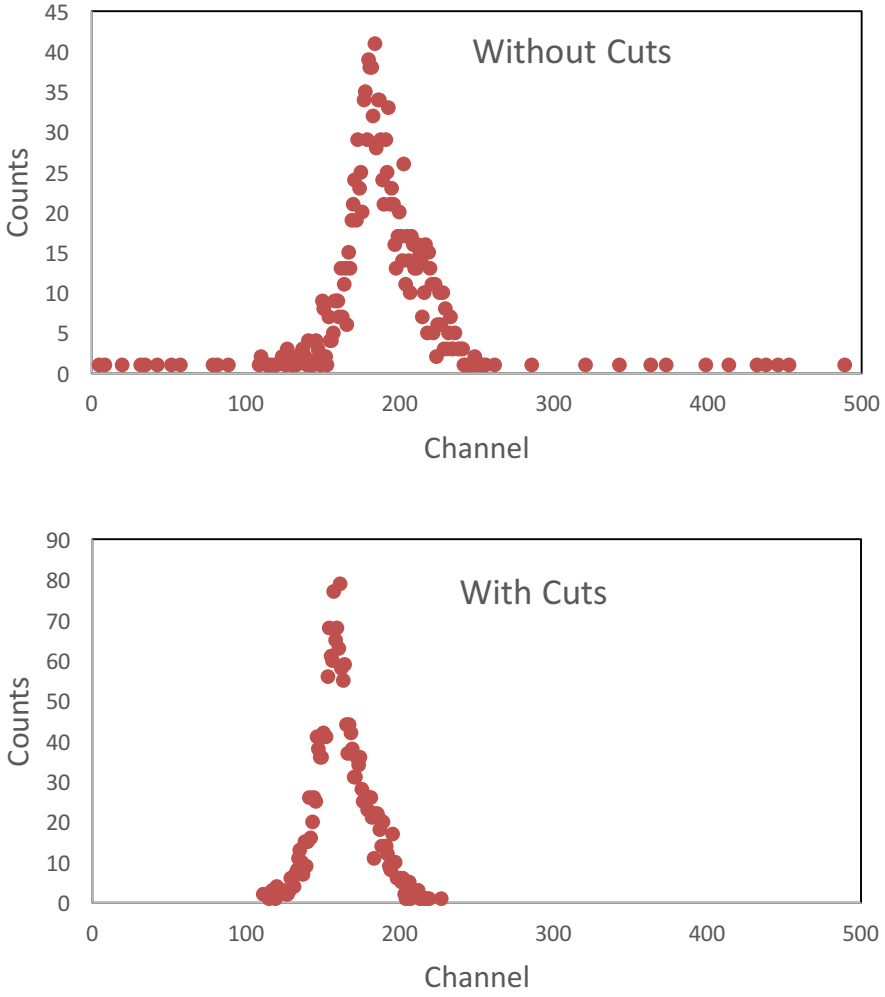

Figure 20. Uncalibrated histograms of the timing difference of coincident beta and gamma pulses. The histogram on the top shows the output of the TPHC recoded using an MCA without cuts. The histogram on the bottom shows the output of the TPHC for only pulses that fell within the range of the SCA window.

4.3. Beta Detector

It was important to know that the TPHC was in fact triggering on real beta pulses and not low energy background or PMT noise. To ensure this was the case, a spectrum was

measured of the ^{60}Co source using the Si detector, shown in Figure 21. The spectrum shows a spike at low energies, suggesting the presence of significant noise. The measurement was repeated with the addition of a linear gate, the electronics diagram of which is shown in Figure 22. The linear gate was added to select for only pulses above the CFD threshold. The resulting spectrum is also shown in Figure 21. The gated spectrum shows no spike like the previous spectrum, suggesting that the CFD is triggering on real beta events.

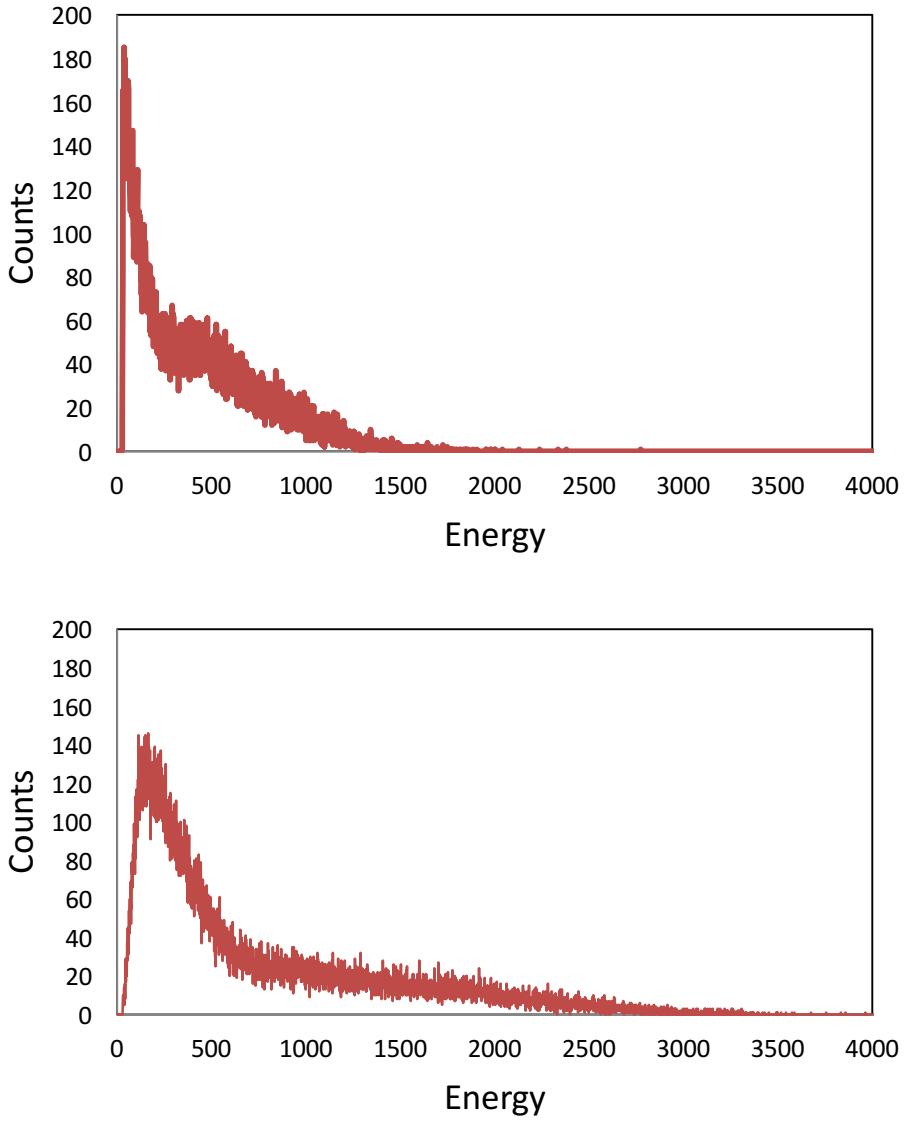

Figure 21. Uncalibrated ^{60}Co beta spectra taken using the Si detector. The spectrum on the top was taken with the discriminator of the CFD set as low as possible (0.05 V). The spectrum on the bottom was taken with the CFD discriminator set to 0.2 V.

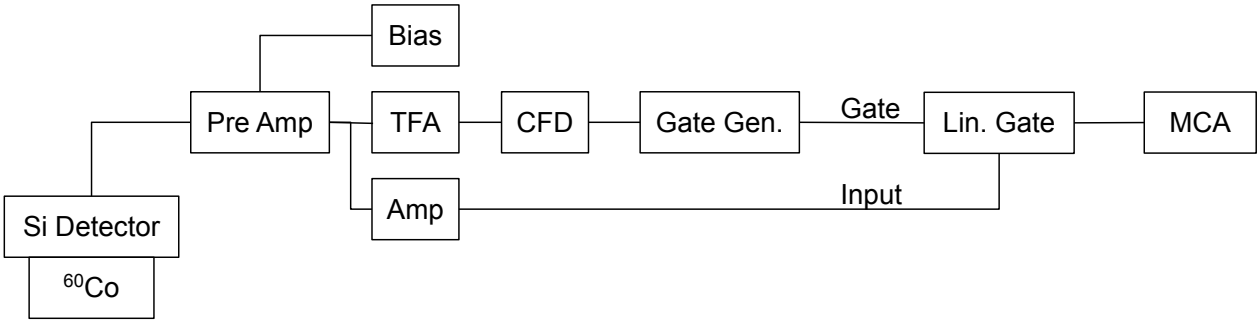

Figure 22. Electronics block diagram used to determine CFD discriminator threshold. The circuit discards beta pulses below the CFD discriminator threshold, which was set to 0.2 V.

To determine if the spectrum obtained using the Si detector matches the ^{60}Co beta spectrum, another spectrum of the ^{60}Co source was taken, shown in Figure 23. This spectrum was calibrated using a ^{207}Bi source, the spectrum of which is shown in Figure 24, which has two very distinct mono-energetic electron peaks at 481.7 keV and 975.7 keV. These emitted electrons are not a result of beta decay but instead result from electron capture by the nucleus followed by internal conversion, allowing for the emission of mono-energetic electrons. As shown in Figure 23, the endpoints of the ^{60}Co spectrum were approximately at the characteristic 310 keV and 1480 keV endpoints characteristic of ^{60}Co, showing that detector was in fact detecting true beta pulses.

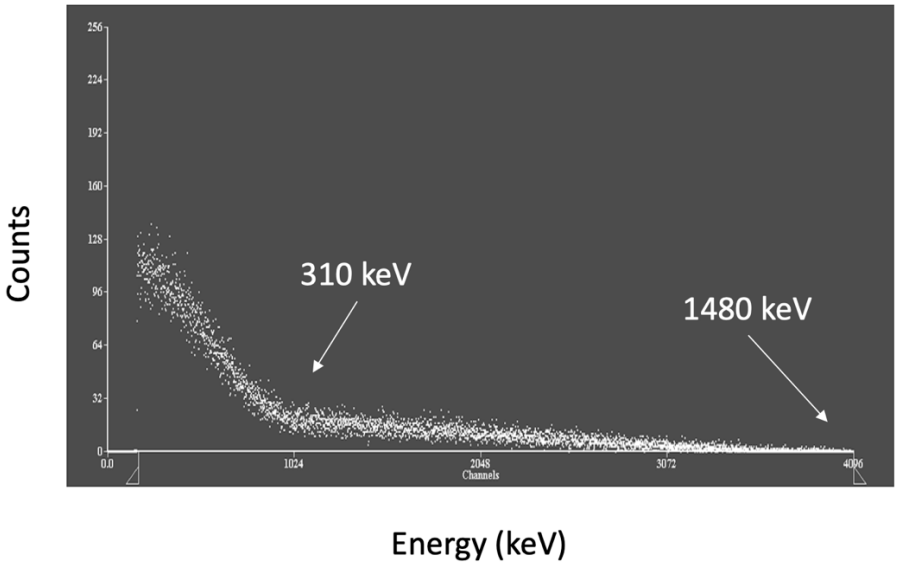

Figure 23. Beta spectrum of ^{60}Co taken using a Si detector. The discriminator discarded low energy pulses due to a high amount of noise. The spectrum exhibited endpoint energies at approximately 310 keV and 1480 keV, which are characteristic of ^{60}Co.

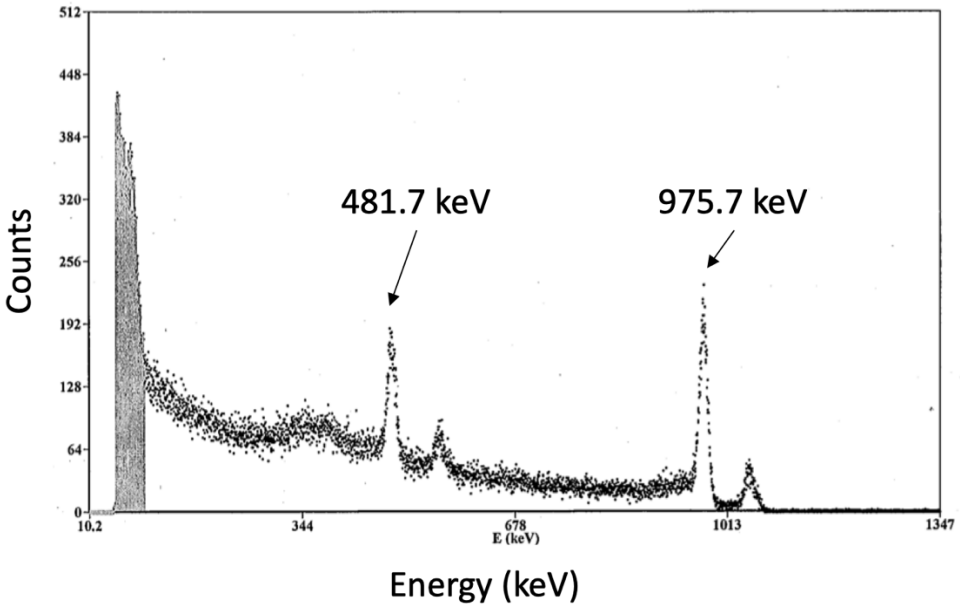

Figure 24. Beta spectrum of ^{207}Bi taken using a Si detector. The two mono-energetic peaks at 481.7 keV and 975.7 keV were used to calibrate the spectrum from the ^{60}Co source.

4.4. Gamma Detector

As explained in Chapter 3, the output of MCA 3 shown in Figure 16 is a gamma spectrum for gamma rays in coincidence with beta particles emitted in the opposite direction. First, a singles gamma spectrum of ^{60}Co was measured to ensure that gamma pulses from the source were actually being detected. As shown in Figure 25, a NaI detector was used to take a singles gamma spectrum of the source, which showed the characteristic 1.17 MeV and 1.33 MeV peaks of ^{60}Co.

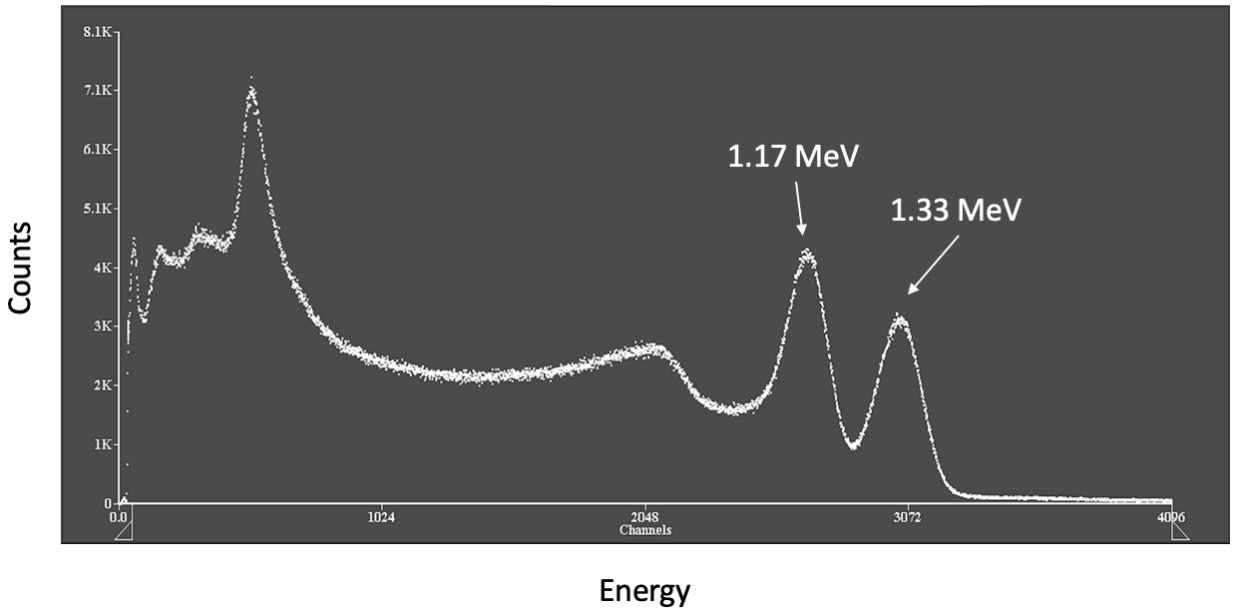

Figure 25. Singles gamma spectrum of ^{60}Co taking using a NaI detector. The 1.17 MeV and 1.33 MeV peaks can be seen.

With both the gamma and beta detectors determined to be triggering on real pulses, a coincidence spectrum could be taken to ensure that the electronics were working as expected. Shown in Figure 26 is a coincidence gamma spectrum taken using a NaI detector. The source was sandwiched between both detectors with the magnet removed to increase the count rate. The resulting spectrum was a ^{60}Co gamma spectrum as expected, showing that the electronic delays were set correctly to accept true gamma pulses.

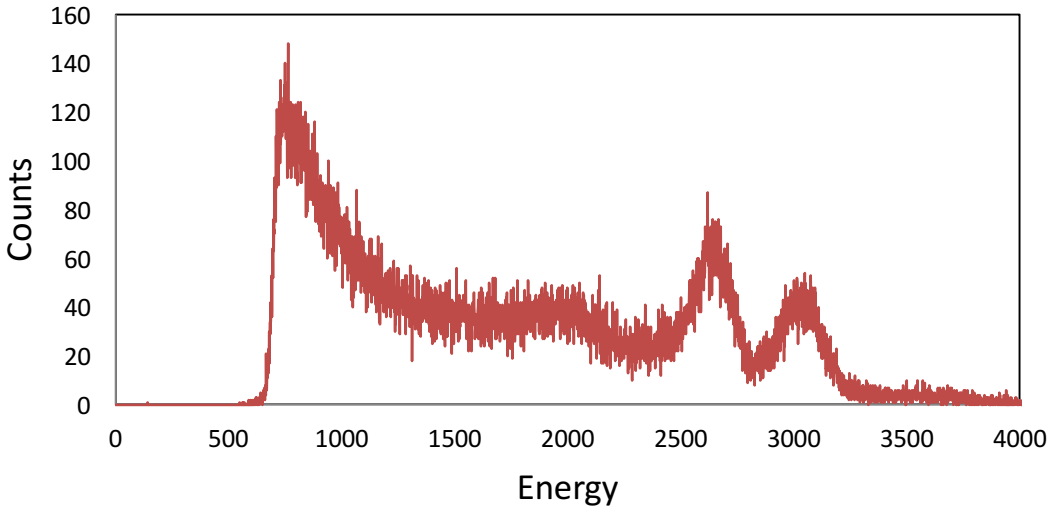

Figure 26. Coincidence gamma spectrum of ^{60}Co using a NaI detector. Two distinct gamma peaks at 1.17 MeV and 1.33 MeV can be seen. Data collection was over a period of 18.5 hours.

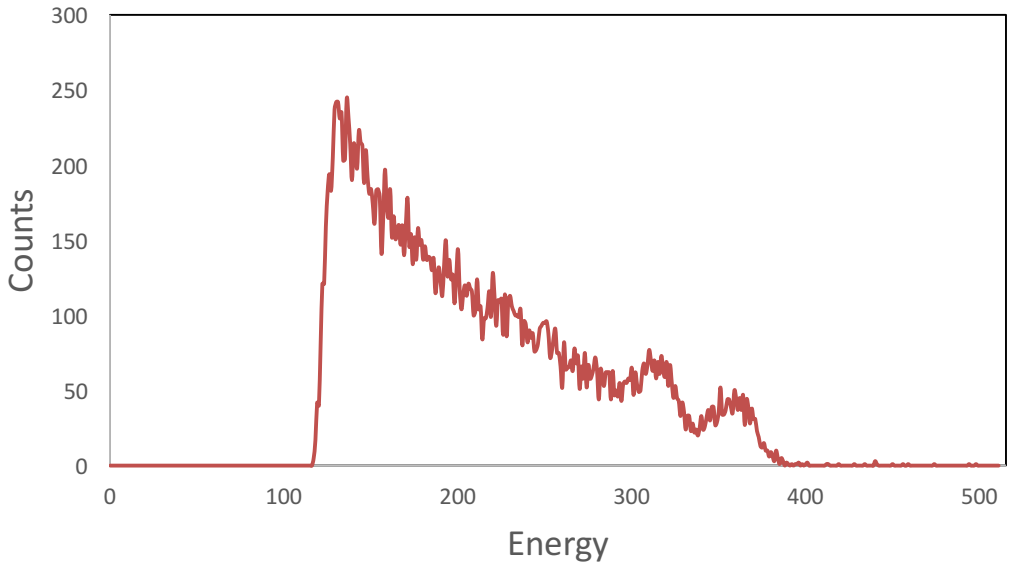

Figure 27. Coincidence gamma spectrum of ^{60}Co with the magnet between the source and the NaI gamma detector. The magnet was not energized, and data were collected for almost 6 days. Two distinct gamma peaks can be seen, showing that the count rate is high enough to be seen above the background.

Next, the magnet was placed back in between the ^{60}Co source and a NaI detector, and a coincidence spectrum was recorded with the magnet off, meaning no magnetic field was generated. Shown in Figure 27 is the coincidence spectrum with the magnet in place but turned off. The two ^{60}Co gamma peaks can still be seen, showing that the coincidence count rate is high enough to be seen above the background.

Unfortunately, it was discovered that when the magnet was turned on, the magnetic field produced was large enough to disrupt the photomultiplier tube (PMT) of the NaI detector. The PMT amplifies the signal using an electron cascade through a series of dynodes. Obviously, the path of these electrons becomes altered in a magnetic field, which in this case resulted in no signal being detected when the magnet was on.

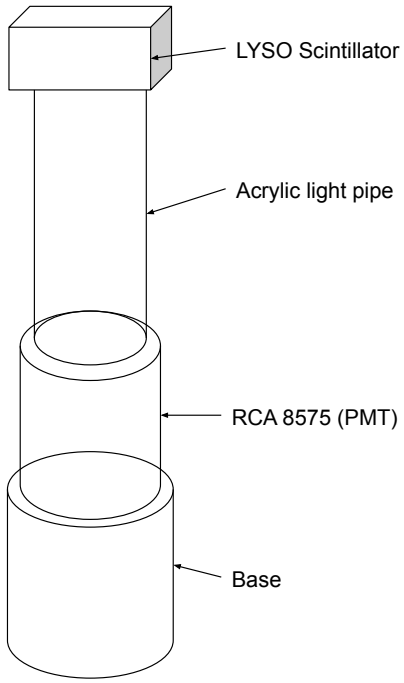

Figure 28. New detector design which allows the PMT to be farther away from the magnet. A scintillator crystal is attached to an acrylic light pipe which carries the signal to the PMT. The crystal and light pipe are covered in foil and black electrical tape to ensure that the detector is light tight (not pictured).

As a result, the experimental design which placed a NaI detector directly below the magnet needed to be modified. It was decided to construct a new detector which used a light guide, such as an acrylic rod, to allow the PMT to be farther away from the magnetic field. A

diagram of the new detector design is shown in Figure 28. Because NaI is extremely hygroscopic and must be hermetically sealed in a container, a new scintillator crystal needed to be used with the new detector.

Several scintillation materials were tested for the new detector to ensure that they had a high enough energy resolution for the experiment. First, a LYSO crystal was tested. LYSO is a Cerium doped Lutetium based scintillation crystal which has a fast decay time, high density, and is non-hydroscopic [13], all of which is advantageous for gamma detection. However, the LYSO crystal contains a naturally occurring radioactive isotope of Lutetium, ^{176}Lu, which is a beta emitter. The decay of ^{176}Lu also results in the emission of three gamma rays of 307, 202, and 88 keV, which can be self-absorbed and are detected by the crystal. Figure 29 shows the measured self-detecting gamma spectrum produced by the LYSO crystal. Because the ^{60}Co gamma peaks occur at 1.17 and 1.33 MeV, it was thought that this self-detection would not be a problem because the self-detection gamma rays are so much lower in energy. However, Figure 29 shows that the low intensity ^{60}Co gamma peaks had significant background from the ^{176}Lu as well as lower energy resolution. The ^{60}Co spectrum was measured with the source directly above the detector. When the magnet was placed in between the ^{60}Co source and the detector, no ^{60}Co gamma peaks could be distinguished from the background.

For this reason, it was determined that LYSO was not suitable for this application. Next, a Bismuth Germanate (BGO) crystal scintillator was tested. BGO ($Bi_4Ge_3O_{12}$) is a high Z material due to the high atomic number of bismuth (83). Because of its high atomic number and high density (7.13 $g \cdot cm^{-3}$), it is a very efficient gamma ray absorber [14]. Figure 30 shows the ^{60}Co gamma spectrum taken using the assembled BGO detector. Only one gamma peak is visible instead of the expected two different energy peaks, but this is a result of the low energy resolution of the detector. Distinguishing between the two different energy peaks is not necessary for this experiment because the total count rate over the energy range of both peaks is compared when the electron spins are polarized in opposite directions.

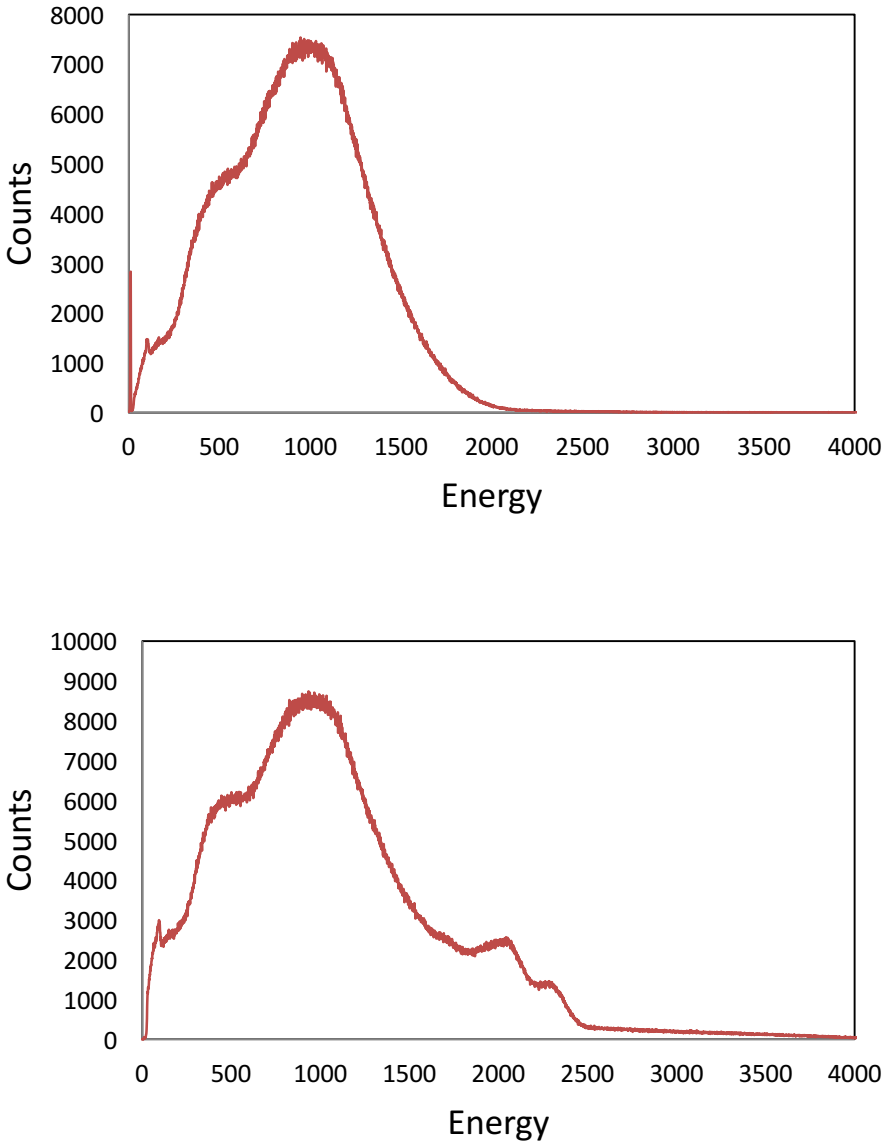

Figure 29. Gamma spectra using LYSO crystal. The top spectrum is the self-detecting gamma spectra resulting from the decay of ^{176}Lu. The bottom spectrum is the gamma spectrum of ^{60}Co taken using the LYSO crystal. The two ^{60}Co gamma peaks contain significant background from ^{176}Lu. For each spectrum, the ^{60}Co source was placed directly on top of the detector and data was recorded for 12 minutes.

Next, a coincidence spectrum was taken to determine if the BGO detector would afford a high enough count rate that a gamma peak could still be seen after transmission through the magnet. Figure 31 shows the ^{60}Co coincidence spectrum measured with the magnet between the source and the BGO detector. No distinct gamma peak can be seen above the

background. This means that the BGO detector energy resolution is inadequate for this measurement unless modifications are made.

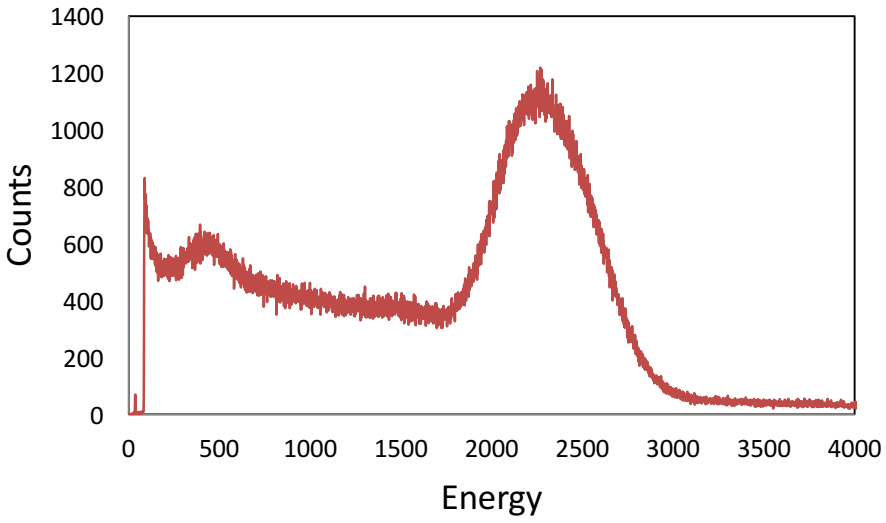

Figure 30. Singles gamma spectrum of ^{60}Co taken using the BGO detector. Only one gamma peak is visible due to the low energy resolution of the detector.

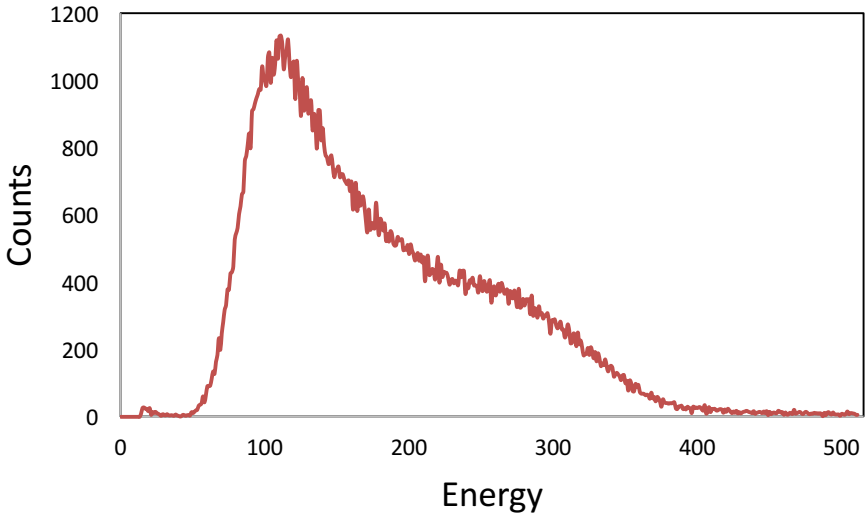

Figure 31. Coincidence gamma spectrum of ^{60}Co with the magnet between the source and the BGO gamma detector. The magnet was not on, and data were collected for 7.3 days. The gamma peaks cannot be seen above the background.

4.5. Count Rate and Efficiency of Experiment

The absolute efficiency of the NaI detector is given by,

$$\text{abs eff} = \frac{\text{count rate}}{\text{activity}}. \tag{19}$$

We know that for each decay two gamma rays are emitted (99.88% of the time), so the count rate was measured to be 11.6 counts/second for the 1.33 MeV peak. For this measurement, the magnet was removed but the ^{60}Co source was suspended 9.27 cm (thickness of magnet) above the face of the NaI detector to maintain the same solid angle. Because the source was electroplated about 6 years ago with an activity of approximately 1 μCi, the activity of the ^{60}Co source was assumed to be 0.5 μCi (1850 decays/second) because the half-life of ^{60}Co is 5.26 years, giving the NaI detector an absolute singles efficiency of approximately 0.63%. This efficiency is extremely low, suggesting that the activity of the source was actually much less than 0.5 μCi.

To estimate the absolute efficiency of the Si detector, the count rate in the entire beta spectrum was measured, because every decay emits one beta particle. The measurement was taken with the source directly below the detector. Because the discriminator threshold was set to a beta energy of approximately 50 keV, this estimate is expected to be low. The count rate was 144 counts/second, resulting in an absolute singles efficiency of about 7.8%.

The energy resolution of the NaI detector was measured using the full width half maximum (FWHM) to be 7.6% for the 1.33 MeV peak and 9.5% for the 1.17 MeV peak, which is typical for a 2 inch NaI detector.

The percent transmittance of the gamma rays through the magnet was calculated using,

$$I = I_o e^{-\mu x}, \tag{20}$$

where I_o is the initial intensity of the gamma rays and I is the intensity after traveling a distance x through the material. The linear attenuation coefficient, μ, is dependent on energy of the incident gamma rays and on the material that the gamma rays travel through. Because the gamma rays have energies of 1.17 and 1.33 MeV, the average of the two

energies, 1.25 MeV, was used. The magnet has a 9.27 cm thick steel core, which results in approximately 2.0% transmission of 1.25 MeV gamma rays using the linear attenuation coefficient of iron (0.421 cm^{-1}), which is a surprisingly small fraction.

To confirm these calculations, two gamma spectra were taken with the NaI detector 9.27 cm away from the source: one with the magnet in place and one without. The count rate was determined by using the total counts over both gamma energy peaks, and the percent transmittance was found to be 1.95%, in good agreement with the calculated 2.0%.

Using Equation (14), the collection time for the current setup can be estimated. To do so, the coincidence count rate without the attenuator in place, R_0, was measured to be approximately 0.0852 counts per second for the 1.33 MeV gamma ray. For a relative uncertainty, $\delta E/E$, of 0.25, this resulted in a collection time of 308 days. The experiment does count gamma rays from both the 1.17 and 1.33 MeV energy peaks, but the measured coincidence count rate also did not subtract out the background, which would reduce the count rate farther and increase the required collection time. Obviously, this setup is currently unacceptable, and needs further modifications.

Shown in Figure 32 is a plot of the collection time as a function of attenuator thickness as expressed in Equation (14) using the current experimental parameters where R_0 is 0.0852 counts per second. The molecular weight of iron, A, is 55.845 $g \cdot mol^{-1}$, the density of the iron core, ρ, is 7.15 $g \cdot cm^{-3}$, the polarization of gamma rays, P, is 1, the number of oriented electrons per atom, v, is 2.06, and the relative uncertainty, $\delta E/E$, is 0.25. For the 1.17 MeV gamma ray, the cross section, σ_c, is -1.457×10^{-26} cm^2 and the mass attenuation coefficient, μ, is 5.893×10^{-2} $cm^2 \cdot g^{-1}$. For the 1.33 MeV gamma ray, the cross section, σ_c, is -1.682×10^{-26} cm^2 and the mass attenuation coefficient, μ, is 5.196×10^{-2} $cm^2 \cdot g^{-1}$. As can be seen in the plot, the optimal attenuator length for a minimized collection time is approximately 5 cm.

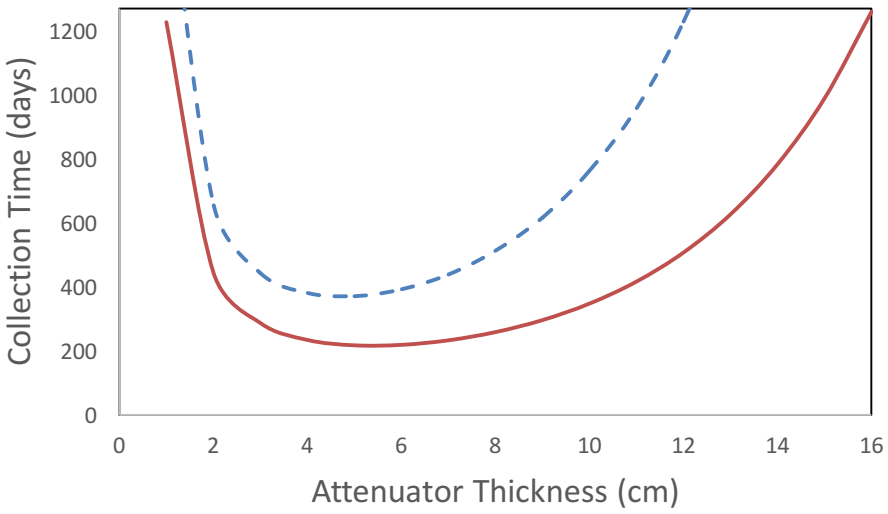

Figure 32. Plot of collection time, in days, as a function of attenuator thickness for a relative uncertainty of 0.25. Both the 1.17 MeV (dashed) and 1.33 MeV (solid) gamma ray energies are plotted. The optimal attenuator thickness is approximately 5 cm to minimize collection time.

Even if the length of the steel attenuator was reduced to the optimal 5 cm length determined by Equation (14), the current setup would still require a collection time of 217 days for a relative uncertainty of 0.25, which is still unacceptable. As a result, R_0, the coincidence rate when the attenuator is not in place, needs to be increased significantly. The easiest way this can be done is by increasing the activity of the source.

To get a better estimate of the current activity of the ^{60}Co source, it was assumed that the solid angle of the Si detector was approximately 33% (θ=70^0), because the source is directly below the detector. With the beta particle count rate of 144 counts per second, this yielded a source activity of approximately 0.012 μC, which is significantly lower than the previously assumed 0.5 μC. If the activity of the source was increased to the maximum exempt source activity of 1 μC [15], that would be a one hundredfold increase, resulting in a collection time of approximately three days, which is much more manageable.

Chapter 5

CONCLUSIONS

5.1. Summary

Parity violation of the weak force is a monumental modern physics discovery. An experiment is being developed at Houghton College to demonstrate this parity violation using a low cost, easy to use procedure and apparatus, as well as materials common to undergraduate physics laboratories. The experiment, using a method originally suggested in the seminal paper by Lee and Yang [1] and taking inspiration from the experiment of Lundby et al. [7], will measure the circular polarization of gamma rays as a way to indirectly measure the difference in the number of right-handed and left-handed beta particles emitted from ^{60}Co. A measured difference in the count rate will show that parity is violated.

5.2. Future Work

Because of the desire to use a low activity source and inexpensive but low energy resolution scintillation detector, the current setup will need further modification before a statistically asymmetry can be measured. The main problem is the coincidence count rate is too low compared to the background rate, making the collection time required to measure a statistically significant asymmetry unacceptably long. There are several ways the count rate can be increased. One obvious way to do this is to make a new source with a higher activity. The increased activity will result in more gamma rays being emitted, meaning an increased number of gamma rays will be transmitted through the steel. As shown in Chapter 4, the activity of the source can be significantly increased and still stay under the maximum exempt source activity of 1 μC.

Another modification that needs to occur that will decrease the collection time is to decrease the thickness of the steel core. Decreasing the thickness of the steel increases the count rate, but it also decreases the number of interactions that the gamma rays have with the electrons in the steel, which decreases the measurable difference in count rate when

the electrons are polarized in opposite directions. As shown in Figure 32, the optimal steel thickness is for this experiment is approximately 5 cm. If the coincidence count rate is increased by both decreasing the thickness of the magnet and increasing the activity, the count rate will be high enough for a statistically significant asymmetry to be measured.

References

[1] T.-D. Lee and C.-N. Yang, Phys. Rev. **104**, 254 (1956).
[2] C.-S. Wu, E. Ambler, R. Hayward, D. Hoppes, and R. P. Hudson, Phys. Rev. **105**, 1413 (1957).
[3] A. Chodos, APS News. **10**, 11 (2001).
[4] M. Gardner, The New Ambidextrous Universe: Symmetry and Asymmetry from Mirror Reflections to Supersymmetry, 3rd Ed. (Dover Publications, Mineola, NY, 2005), pp. 212-213.
[5] The Nobel Prize in Physics 1957 (2020). Retrieved 8 May 2020, from https://www.nobelprize.org/prizes/physics/1957/summary/
[6] Chien-Shiung Wu - Wolf Prize Laureate in Physics 1978 (2020). Retrieved 8 May 2020, from https://wolffund.org.il/2018/12/09/chien-shiung-wu/
[7] A. Lundby, A. Patro, and J.-P. Stroot, Il Nuovo Cimento **6**, 745 (1957).
[8] E. Browne and J. K. Tuli, Nuclear Data Sheets **114**, 1849 (2013).
[9] H. Schopper, Nuc Phys **3**, 158 (1958).
[10] Michael R. Ganger, Undergraduate thesis, Houghton College, 2017.
[11] R. Chesler, Nucl. Instr. Meth. **37**, 185 (1965).
[12] Tyco Electronics Corporation, Potter & Brumfield KHA Series Panel Plug-in Relay Datasheet (2015). http://www.farnell.com/datasheets/1928624.pdf?_ga=2.158450105.2085052670.1550859877-1351201775.1550859877.
[13] Saint-Gobain Crystals, LYSO Scintillation Material (2018). https://www.crystals.saint-gobain.com/sites/imdf.crystals.com/files/documents/lyso-material-data-sheet.pdf
[14] Saint-Gobain Crystals, BGO Scintillation Material (2016). https://www.crystals.saint-gobain.com/sites/imdf.crystals.com/files/documents/bgo-material-data-sheet.pdf
[15] United States Nuclear Regulatory Commission, NRC: 10 CFR 30.71 Schedule B (2017). https://www.nrc.gov/reading-rm/doc-collections/cfr/part030/part030-0071.html